Gating properties of the P2X2a and P2X2b receptor channels: Experiments and mathematical modeling

Anmar Khadra,[1,3] Zonghe Yan,[2] Claudio Coddou,[2] Melanija Tomić,[2] Arthur Sherman,[1] and Stanko S. Stojilkovic[2]

[1]Laboratory of Biological Modeling, National Institute of Diabetes and Digestive and Kidney Diseases, and [2]Section on Cellular Signaling, Program in Developmental Neuroscience, National Institute of Child Health and Human Development, National Institutes of Health, Bethesda, MD 20892

[3]Department of Physiology, McGill University, Montréal, Québec H3A 1Y6, Canada

Adenosine triphosphate (ATP)-gated P2X2 receptors exhibit two opposite activation-dependent changes, pore dilation and pore closing (desensitization), through a process that is incompletely understood. To address this issue and to clarify the roles of calcium and the C-terminal domain in gating, we combined biophysical and mathematical approaches using two splice forms of receptors: the full-size form (P2X2aR) and the shorter form missing 69 residues in the C-terminal domain (P2X2bR). Both receptors developed conductivity for N-methyl-D-glucamine within 2–6 s of ATP application. However, pore dilation was accompanied with a decrease rather than an increase in the total conductance, which temporally coincided with rapid and partial desensitization. During sustained agonist application, receptors continued to desensitize in calcium-independent and calcium-dependent modes. Calcium-independent desensitization was more pronounced in P2X2bR, and calcium-dependent desensitization was more pronounced in P2X2aR. In whole cell recording, we also observed use-dependent facilitation of desensitization of both receptors. Such behavior was accounted for by a 16-state Markov kinetic model describing ATP binding/unbinding and activation/desensitization. The model assumes that naive receptors open when two to three ATP molecules bind and undergo calcium-independent desensitization, causing a decrease in the total conductance, or pore dilation, causing a shift in the reversal potential. In calcium-containing media, receptor desensitization is facilitated and the use-dependent desensitization can be modeled by a calcium-dependent toggle switch. The experiments and the model together provide a rationale for the lack of sustained current growth in dilating P2X2Rs and show that receptors in the dilated state can also desensitize in the presence of calcium.

INTRODUCTION

Purinergic P2X receptors (P2XRs) are a family of ATP-gated receptor channels. Seven mammalian purinergic receptor subunits, denoted P2X1 through P2X7, have been identified (North, 2002). The gating of P2XRs usually consists of three phases: (1) a rapid (millisecond time scale) rising phase of inward current induced by the application of agonist (activation phase), which reflects the passage of monovalent and divalent cations through the channel pore (this is also called the open-1 phase, and the current through this state is termed the I_1 current); (2) a slow and receptor-specific developing decay phase usually follows in the presence of an agonist (desensitization phase); and (3) a relatively rapid decay of current after agonist removal (deactivation phase) (Egan et al., 2006). P2X7R and P2X4R, when expressed in *Xenopus laevis* oocytes and bathed in Ca^{2+}-deficient medium, also exhibit activation-dependent

changes in ion selectivity during sustained agonist application. The opening of the channel pore is accompanied by a secondary current growth that temporally coincides with an additional change on a time scale of seconds in the permeability, when channels also become porous to organic cations, such as $NMDG^+$, and dyes, such as YOPRO-1 and Fura-2 (Surprenant et al., 1996; Khakh et al., 1999; Yan et al., 2008, 2010). The mode of the channels that is permeable to both small and large ions is termed the dilated or open-2 state, and the corresponding current is labeled I_2 (Egan et al., 2006).

A sustained development of permeability for large organic cations and a shift in the reversal potential to more positive voltages have also been observed in cells expressing P2X2R when bathed in $NMDG^+$-containing medium (Virginio et al., 1999; Khakh and Egan, 2005; Chaumont and Khakh, 2008). However, activated P2X2R does not generate I_2, but rather desensitizes slowly during sustained agonist application (North, 2002).

The Rockefeller University Press $30.00
J. Gen. Physiol. Vol. 139 No. 5 333–348
www.jgp.org/cgi/doi/10.1085/jgp.201110716

333

At the present time, it is not clear how P2X2R can take two opposite states, dilated and desensitized states, why the dilated state of the receptor is not accompanied by I_2 growth, and whether the receptor in the dilated state can also desensitize. Furthermore, P2X2R is unique among the seven mammalian receptors because multiple splice variants exist in humans, rats, mice, and guinea pigs and are able to generate homomeric and heteromeric channels with different functional properties (Coddou et al., 2011). The spliced subunit named P2X2b lacks a series of 69 C-terminal amino acids and creates a functional homomeric channel that desensitizes more rapidly than the full-sized receptor, named P2X2a (Brändle et al., 1997; Simon et al., 1997; Koshimizu et al., 1998b). The dilation properties of P2X2bR have not been studied previously. Here, we combine biophysical and mathematical approaches to address these issues.

MATERIALS AND METHODS

Cell culture and transfection
Large-scale plasmid DNAs were prepared using a QIAfilter Plasmid Maxi kit (QIAGEN). Human embryonic kidney (HEK)293 and gonadotropin-releasing, hormone-secreting (GT1) cells were used for the expression of wild-type and mutant receptors, as described previously (Yan et al., 2006). HEK293 cells were routinely maintained in Dulbecco's modified Eagle's medium (DMEM) containing 10% (vol/vol) fetal bovine serum (Invitrogen) and 1% (vol/vol) penicillin-streptomycin liquid (Invitrogen) in a tissue culture incubator. GT1 cells were cultured in DMEM/Ham's F-12 medium (1:1) containing 10% (vol/vol) fetal bovine serum and 100 µg/ml gentamicin (Invitrogen). For electrophysiological measurements, cells were grown on 35-mm dishes at a density of 0.5×10^6 cells per dish, whereas for imaging studies, GT1 cells were grown on 25-mm coverslips placed in 35-mm dishes at a density of 0.10^6 cells per dish. Transfection was conducted 24 h after plating the cells, using 2 µg DNA and 5 µl Lipofectamine 2000 reagent (Invitrogen) in 2 ml of serum-free Opti-MEM. After 4.5 h of incubation, the transfection mixture was replaced with a normal culture medium, and cells were cultured for an additional 24–48 h. For electrophysiological measurements, transfected cells were mechanically dispersed and recultured on 35-mm dishes for 2–10 h.

Current measurements
ATP-induced currents were measured using both the whole cell and the perforated cell mode using amphotericin. Before measurement, amphotericin and the dispersing agent pluronic F-127 from stock solutions were added to the intracellular solution to obtain final concentrations of 250 and 500 µg/ml, respectively. Recordings were performed 10 min after seal formation. In some experiments, both whole cell and outside-out recording modes were used on the same cell. All experiments were done on single cells with an average capacitance of 10 pF at room temperature using an amplifier (Axopatch 200B; Molecular Devices), as described previously (Yan et al., 2006). Unless otherwise stated, membrane potential was held at −60 mV. I-V relations were used to estimate changes in reversal potential during agonist application and were obtained by voltage ramps from −80 to +80 mV twice per second during 50 s. If not otherwise stated, patch electrodes were filled with solution containing 145 mM NaCl, 10 mM

EGTA, and 10 mM HEPES, and cells were bathed in Krebs-Ringer (KR)-like bath buffer containing 147 mM NaCl, 3 mM KCl, 1 mM MgCl$_2$, 2 mM CaCl$_2$, 10 mM glucose, and 10 mM HEPES; the pH was adjusted to 7.35 with 10 M NaOH. Cells with EGFP fluorescence were identified before immersing the electrode in bath solution for gigaohm seal.

Fluorescence imaging
Transfected GT1 cells plated on 25-mm coverslips were bathed in KR medium containing 2.5 µM Fura-FF AM (Invitrogen) for 1 h at room temperature. After the coverslips were washed with dye-free KR media, they were mounted on the stage of a microscope (Axiovert 135; Carl Zeiss) attached to an Attofluor Digital Fluorescence Microscopy System (Atto Instruments). Cells were examined under a 40× oil-immersion objective during exposure to alternating 340- and 380-nm excitation beams, and the intensity of light emission at 520 nm (F_{340} and F_{380}) was followed in several single cells simultaneously.

Mathematical model
We designed a mathematical model to account for three key properties of P2X2R: (1) opening and dilation in response to stimulation by ATP; (2) desensitization; and (3) increased rate of desensitization when intracellular calcium concentration ($[Ca^{2+}]_i$) increases. In Fig. 1, we show a Markov state (minimal) model consisting of 16 states arrayed in four rows that accomplishes these goals. Each state corresponds to the fraction of P2X2R that is bound to up to three ligand (ATP) molecules. The state C_1 in the second row (counting from the top) represents a naive state not previously exposed to ATP stimulation. The second row governs receptor opening via the states Q_1 and Q_2, both possessing the same conductance g_{12}. The third row, on the other hand, controls receptor dilation via Q_3 and Q_4, both possessing the same conductance g_{34}. In other words, the scheme requires at least two ATP molecules to be bound to the receptor for the channel to open and dilate. The two middle rows correspond to our previous model developed for P2X7 (Yan et al., 2010), but with faster dilation and no long-term memory state of sustained current. Here, maintained stimulation instead results in a mild and slow desensitization, governed by the top row. When $[Ca^{2+}]_i$ increases, the rate of desensitization is markedly increased, which is governed by the bottom row.

Thus, receptors in states C_1, C_4, D_1, and D_1^c have no ATP bound, receptors in states C_2, C_3, D_2, and D_2^c have one ATP bound, receptors in states Q_1, Q_4, D_3, and D_3^c have two ATP bound, and receptors in states Q_2, Q_3, D_4, and D_4^c have three ATP bound; ATP binding is indicated by the white and black circles on each state. The states C_i, D_i, and D_i^c (i = 1,2,3,4) correspond to receptors with closed channel pores, whereas those in states Q_i have open pores. In addition, Q_3 and Q_4 are dilated, with conductance g_{34} greater than the conductance g_{12} of Q_1 and Q_2. Forward rates are dictated by the number of unoccupied sites, ATP concentration (A), and the transition rate k_2, whereas backward rates are dictated by the number of occupied sites and transition rate k_1. Receptors in the states D_i and D_i^c are desensitized via the Ca^{2+}-independent and Ca^{2+}-dependent pathways, respectively. Because Ca^{2+}-dependent desensitization is not observed at low ATP concentration, reaching state Q_3 is required for this pathway to occur (at rate L_2), unlike the Ca^{2+}-independent desensitization, which requires at most one bound ATP to occur (at rates L_1 and L_3). Desensitized receptors with no ATP bound (i.e., states D_1 and D_1^c) return back to the naive state C_1 at rate L_1 (via C_4 for the latter). The transitions between states Q_2 and Q_3 are assumed to be slow (governed by the rates L_4 and L_5), especially in NMDG$^+$-only–containing medium; this is necessary to capture the shift in reversal potential over several seconds observed during voltage-ramp experiments.

Corresponding to the scheme of Fig. 1 is the following system of 16 linear ordinary differential equations:

$$\frac{dD_1}{dt} = k_1 D_2 - (3k_2 A + L_1)D_1 \qquad (1)$$

$$\frac{dD_2}{dt} = 3k_2 A D_1 + 2k_1 D_3 + L_1 C_2 - (k_1 + 2k_2 A)D_2 \qquad (2)$$

$$\frac{dD_3}{dt} = 2k_2 A D_2 + 3k_1 D_4 + L_1 Q_1 - (2k_1 + k_2 A)D_3 \qquad (3)$$

$$\frac{dD_4}{dt} = k_2 A D_3 + L_3 Q_2 - 3k_1 D_4 \qquad (4)$$

$$\frac{dC_1}{dt} = k_1 C_2 + L_1(D_1 + C_4) - 3k_2 A C_1 \qquad (5)$$

$$\frac{dC_2}{dt} = 3k_2 A C_1 + 2k_1 Q_1 - (k_1 + 2k_2 A + L_1)C_2 \qquad (6)$$

$$\frac{dQ_1}{dt} = 2k_2 A C_2 + 3k_1 Q_2 - (2k_1 + k_2 A + L_1)Q_1 \qquad (7)$$

$$\frac{dQ_2}{dt} = k_2 A Q_1 + L_5 Q_3 - (3k_1 + L_3 + L_4)Q_2 \qquad (8)$$

$$\frac{dC_4}{dt} = k_1 C_3 + L_1 D_1^c - (3k_2 A + L_1)C_4 \qquad (9)$$

$$\frac{dC_3}{dt} = 3k_2 A C_4 + 2k_1 Q_4 - (k_1 + 2k_2 A)C_3 \qquad (10)$$

$$\frac{dQ_4}{dt} = 2k_2 A C_3 + 3k_1 Q_3 - (2k_1 + k_2 A)Q_4 \qquad (11)$$

$$\frac{dQ_3}{dt} = k_2 A Q_4 + L_4 Q_2 - (3k_1 + L_2 + L_5)Q_3 \qquad (12)$$

$$\frac{dD_1^c}{dt} = k_1 D_2^c - (3k_2 A + L_1)D_1^c \qquad (13)$$

$$\frac{dD_2^c}{dt} = 3k_2 A D_1^c + 2k_1 D_3^c - (k_1 + 2k_2 A)D_2^c \qquad (14)$$

$$\frac{dD_3^c}{dt} = 2k_2 A D_2^c + 3k_1 D_4^c - (2k_1 + k_2 A)D_3^c \qquad (15)$$

$$\frac{dD_4^c}{dt} = k_2 A D_3^c + L_2 Q_3 - 3k_1 D_4^c. \qquad (16)$$

The desensitization rate L_2 depends on the temporal dynamics of $[Ca^{2+}]_i$, which is needed to account for the increased rate of desensitization in response to repetitive stimulation with ATP. Moreover, once rapid desensitization is established, it persists in the face of ATP removal and reapplication. This feature indicates that L_2 has memory for exposure to high $[Ca^{2+}]_i$. In the absence of data for the molecular basis of this memory, we model it phenomenologically as a toggle switch (Tyson et al., 2003), which depends on both $[Ca^{2+}]_i$ through positive feedback and the concentration of an unknown molecule X through negative feedback. The positive and negative feedbacks combine to produce bistability (hysteresis), which is responsible for generating the memory effect.

Three auxiliary equations are needed for the dynamics of $[Ca^{2+}]_i$ responsible for desensitization. The equation for L_2 consists of two terms: an activation term (the backward N-shaped curve in Fig. 2 A), which shifts upward as $[Ca^{2+}]_i$ increases, and a linear inhibition term governed by X. The resulting equation for L_2 is then

$$\frac{dL_2}{dt} = \beta_1 [Ca^{2+}]_i \frac{\beta_2 + (L_2^* - L_2)^2}{\beta_3^2 + (L_2^* - L_2)^2} - \beta_4 X L_2, \qquad (17)$$

where $\beta_1, \beta_2, \beta_3, \beta_4, L_2^*$ are constants (values shown in Table 1). We emphasize that we opted for this formalism rather than a Hill function to describe the effect of $[Ca^{2+}]_i$, because the latter (a) would require a Hill coefficient of at least $n = 7$, which seems implausible, to capture all the experimental results, and, more important, (b) would not generate bistability and memory.

The equation for the concentration of the unknown inhibiting agent X consists of a constant source, σ, and linear degradation, $k_x X$:

$$\frac{dX}{dt} = \sigma - k_x X. \qquad (18)$$

The free $[Ca^{2+}]_i$ follows a simple mass balance equation consisting of a flux term caused by channel opening and a small efflux term:

$$\frac{d[Ca^{2+}]_i}{dt} = -f(\alpha S R I + k_c [Ca^{2+}]_i), \qquad (19)$$

where f is the fraction of free $[Ca^{2+}]_i$, α is Faraday's constant, S is the fraction of the current, I is attributable to calcium, R converts the units of current from A to pA, and k_c is the efflux rate. Note that receptors are overexpressed in our cell lines so efflux, which depends on the native Ca^{2+} pumps, is much weaker and slower than influx. All the variables stated above start from zero initial conditions, except for the naive state C_1, which starts at $C_1(0) = 1$. The whole cell current is given by

$$I = g_{12}(Q_1 + Q_2)(V - E_{12}) + g_{34}(Q_3 + Q_4)(V - E_{34}), \qquad (20)$$

where E_{12} and E_{34} are the reversal potentials of the open states (Q_1, Q_2) and dilated states (Q_3, Q_4), respectively, and V is the holding potential. Parameter values (for P2X2aR, P2X2bR, and NMDG$^+$- and Na$^+$-only containing media) are listed in Table 1.

The backward N-shaped curves in Fig. 2 A are the L_2 nullclines, which represent the steady states of Eq. 17 for L_2 as a function of X. The nullcline is plotted for three different values of $[Ca^{2+}]_i$ (Fig. 2 A): solid, 0.1 mM; dashed, 1 mM; dotted, 32.6 mM. Similarly, the gray curve is the X nullcline, which is horizontal because L_2 does not appear in Eq. 18, and hence the steady states of X do not depend on L_2. At the intersections of L_2 and X nullclines, both L_2 and X are at steady state. As shown in Fig. 2 A, increasing $[Ca^{2+}]_i$ changes the number of steady states from one to three and then

back to one. The steady states of L_2 with respect to $[Ca^{2+}]_i$ and their stability are summarized in Fig. 2 B. The upper and lower branches (Fig. 2 B, solid) of the S-shaped curve are the stable (physically realizable) steady states, and the middle branch (dashed) consists of unstable steady states, which act as threshold values. For a range of $[Ca^{2+}]_i$ values (from just below 1 µM to just above 10 µM), there are two stable states with low and high values of L_2 and hence desensitization rates. This is what allows the system to act as a toggle switch.

Software
Nonlinear curve fitting of the desensitization phases of currents was performed with the Clampfit 10.0 (Molecular Devices) predefined monoexponential function ($f(t) = B \exp(-t/\tau)$). Concentration–response relationships were fitted to a four-parameter logistic equation ($g(A) = \varphi A^{n_H} / (K^{n_H} + A^{n_H})$) using a nonlinear curve-fitting program, which derives the EC_{50} (K) and Hill's values (n_H) (Kaleidagraph; Synergy Software). The kinetic model was analyzed by phase plane methods, linear stability analysis, and bifurcation methods. Time series simulations and bifurcation diagrams were generated using XPPAUTO (written by Bard Ermentrout and freely available online), and plots of I-V curves were produced using MATLAB (MathWorks).

Online supplemental material
The online supplemental material contains additional experimental and modeling data. Table S1 provides a summary of how sensitive the kinetic model, Eqs. 1–20, is to perturbations in certain key parameters. Fig. S1 shows experimental data on whole cell current recording in cultures bathed in NMDG+ medium. Fig. S2 shows the increasing rate of desensitization caused by the toggle switch during repetitive stimulation. Fig. S3 shows the dose–response curves of current amplitude, current plateau, and percentage of desensitized receptors in accordance with the kinetic model, Eqs. 1–20, during third ATP stimulation of both P2X2aR- and P2X2bR-expressing model cells. Fig. S4 examines the effects of perturbing the parameters of Eq. 17, on the structure of the toggle switch. A brief mathematical analysis is provided to explain the shift in reversal potential and the decrease in the slopes of the I-V curves observed during voltage-ramp experiments. The online supplemental material is available at http://www.jgp.org/cgi/content/full/jgp.201110716/DC1.

RESULTS

Kinetics of P2X2R pore dilation
HEK293 cells expressing P2X2aR, P2X2bR, or P2X4R were bathed in medium containing 155 mM NMDG+, 10 mM HEPES, and 10 mM glucose, and whole cell recording mode was used to study the permeability of these receptors to NMDG+. The pipette contained the default solution, 145 mM NaCl, 10 mM EGTA, and 10 mM HEPES. In one series of experiments, cells were steadily clamped at −60 mV and stimulated with 100 µM ATP
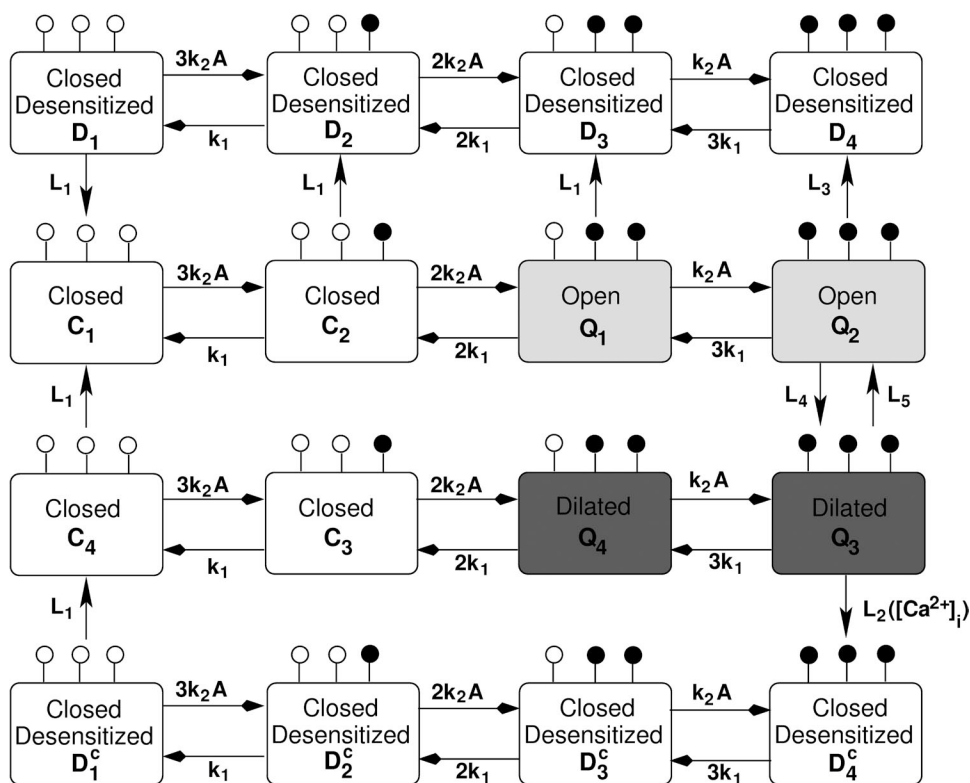

Figure 1. Markov state model describing the binding and unbinding of ATP to P2X2a and P2X2b receptors. The model, Eqs. 1–16, was developed from the scheme for P2X7 (Yan et al., 2010). Each state in this scheme represents the fraction of receptors that belong to a given state. C_i, i = 1,2,3,4, are closed states, whereas Q_1, Q_2 (with conductance g_{12}) are open states, and Q_3, Q_4 (with conductance g_{34}) are dilated states; i.e., their conductances satisfy $g_{12} < g_{34}$. The states D_i (top row), i = 1,2,3,4, are the Ca^{2+}-independent desensitized states, whereas the states D_i^c (bottom row) are the Ca^{2+}-dependent desensitized states. Open circles on each state represent unoccupied ATP-binding sites, and closed circles represent occupied sites. The forward and backward rates in the top and bottom rows (i.e., the desensitized rows) are identical to those in the middle rows. L_i, i = 1,2,3,4,5, are the transition rates between the four rows, where L_4, L_5 are the rates of transition between open and dilated states, and L_1, L_2, L_3 are the desensitization rates. Note that L_2 depends on $[Ca^{2+}]_i$ via the toggle switch shown in Fig. 2.

(Fig. 3 A). Because the holding potential was more positive than the reversal potential for Na$^+$, an initial outward current developed rapidly after agonist application, reflecting an outward movement of intracellular Na$^+$ through the channel pore. This was followed by a decline in current and, in the case of P2X2aR and P2X2bR, a shift from outward to inward current; such a shift was not observed in cells expressing P2X4R. In P2X2aR-expressing cells, the peak amplitude of inward current was reached within 10 s, followed by a modest and slow desensitization. In P2X2bR-expressing cells, the peak amplitude of inward current was reached more rapidly (within 2–3 s) and the decrease in the current amplitude was faster and more profound, culminating in almost complete receptor desensitization within 60 s of agonist application. Under these ionic and recording conditions, P2X4R also desensitized almost completely and much more rapidly than P2X2bR.

In another series of experiments, repetitive 485-ms voltage-ramp pulses from −80 to +80 mV were delivered twice per second from a holding potential of 0 mV (Fig. 3 B). Under these experimental conditions, we detected a shift in reversal potential, indicative of pore dilation, over the course of 6 s from −69 mV to a steady-state level of −9 mV in cells expressing P2X2aR

(Fig. 3 B, left). The temporal correlation between current and changes in reversal potential is shown in Fig. 3 A (inset). Because the shift from outward to inward current in cells expressing P2X2bR was very rapid (Fig. 3 A, middle), we used 48.5-ms voltage ramps twice per 100 ms. Such a protocol allowed detection of a 2–3-s shift from −69 to −5 mV (Fig. 3 B, middle). Consistent with the recording at a steady holding potential (Fig. 3 A, right), no shift in reversal potential was observed in P2X4R-expressing cells (Fig. 3 B, right).

In our experimental conditions, HEK293 cells do not express P2XRs endogenously but do express Ca^{2+}-mobilizing G protein–coupled P2 receptors (P2YRs) (He et al., 2003). To exclude the possible contribution of these receptors to P2X2R dilation, we used GT1 cells, which do not express either P2XRs or P2YRs endogenously (Koshimizu et al., 1998b), and examined the leak of Ca^{2+} dye Fura-2 from cells as an indicator of pore dilation. To eliminate changes in fluorescence induced by Ca^{2+} influx, cells were bathed in Ca^{2+}-deficient KR medium. Under such ionic conditions, there was a progressive decrease in fluorescence intensities at 340 and 380 nm in response to 100-μM ATP application (Fig. 3 C). In cells expressing P2X2aR and P2X2bR, changes in fluorescence intensity occurred in two phases: a rapid

TABLE 1
Parameter values used in the kinetic model of P2X2R gating

Symbol	P2X2a values	P2X2b values	NMDG-only medium	Na-only medium
k_1	1 s^{-1}			
k_2	60,000 (M · s)$^{-1}$			
L_1	0.01 s^{-1}			
L_2*	0.2 s^{-1}	0.3 s^{-1}		
L_3	0.6 s^{-1}		0.3 s^{-1}	0.15 s^{-1}
L_4	0.3 s^{-1}			
L_5	0.004 s^{-1}	0.1 s^{-1}	0.004, 0.1 s^{-1a}	
β_1	100 (s^{-2} · μM^{-1})			
β_2	0.8 s^2			
β_3	0.02 s			
β_4	2 (s · μM)$^{-1}$	0.2 (s · μM)$^{-1}$		
σ	0.04 μM/s			
k_x	0.1 s^{-1}			
f (fraction of free calcium)	0.01^b		0^b	0^b
α (converting current to flux)	5 × 10^{-6} μM/(s · pA)			
S ([Ca^{2+}]$_i$ contribution)	10^{-3b}			
R (converting A to pA)	10^{12b}			
k_c	0.04 s^{-1}			
g_{12} (Q$_1$ and Q$_2$ conductances)	8 × 10^{-8} A			
g_{34} (Q$_3$ and Q$_4$ conductances)	1.2 × 10^{-7} A			
V (holding potential)	−0.06 V			−0.06 or 0.06 V
E$_{12}$ (reversal potential of Q$_1$ and Q$_2$)	−0.02 V		−0.075 V	−0.004 V
E$_{34}$ (reversal potential of Q$_3$ and Q$_4$)	0.02 V		−0.009 V	−0.002 V
WP (washout period)	250 s		NA	NA

Parameters with no values under P2X2bR, NMDG, and Na columns are identical to those listed under the P2X2aR column. NA, not applicable.
[a]Left value is for P2X2aR, and right value is for P2X2bR.
[b]Parameters without units are dimensionless.

phase, followed by a sustained linear phase. In the case of P2X4R-expressing cells, only a slow phase was observed. We interpreted the rapid phase as pore dilation–mediated leak of Fura-2 and the slow phase as dilution of the dye in the cytosol caused by a progressive increase in cell volume occurring at the same rate.

Both the shift in the reversal potential and the leak of Fura-2 were also observed in cells bathed in the presence of 50 µM carbenoxolone, a blocker of pannexin and connexin channels (not depicted). This indicates that development of permeability of cells to NMDG$^+$ and leak of fluorescent dye do not reflect integration of these channels in P2X2R signaling, a finding consistent with a previous report (Chaumont and Khakh, 2008).

With P2X4R, a decrease in the slopes of the I-V curves was observed (Fig. 3 B, right), indicating a decrease in the total conductance and reflecting receptor

Figure 2. The toggle switch responsible for the change from slow to fast desensitization observed in P2X2aR and P2X2bR during repetitive ATP stimulation. The nullclines (A) and the steady states (bifurcation diagram) (B) of subsystem 13–14, obtained by making [Ca^{2+}]$_i$ a parameter, are shown. The X nullcline (gray line) in A intersects the L_2 nullcline initially at one stable steady state when [Ca^{2+}]$_i$ (=0.1 µM) is low (solid line), and then intersects it at three steady states, two of which are stable, when [Ca^{2+}]$_i$ (=1 µM) is intermediate (dashed line), and finally at one stable steady state when [Ca^{2+}]$_i$ (=32.6 µM) is high (dotted line). The changes in the number of steady states are summarized by the S-shaped curve in B, which shows the hysteresis. Stable steady states are shown as solid lines, and unstable steady states are shown as dashed lines; the default values in Table 1 are used. The arrows in B indicate the values of [Ca^{2+}]$_i$ used to plot the L_2 nullclines in A.

desensitization. A decrease in the slopes of the I-V curves was also observed with both P2X2aR and P2X2bR (Fig. 3 B, left and middle), even though a shift in reversal potential shows that the channel is dilating. Such an outcome, also observed by others (Chaumont and Khakh, 2008), may also be caused by receptor desensitization, which could mask the dilation of the channel. To clarify this issue, we performed additional experiments varying holding potentials and bath ion concentrations.

In the experiments illustrated in Fig. 4 A, cells were bathed in NMDG$^+$-containing medium (the same ionic conditions as in Fig. 3, A and B) but held at +60 mV, which increases the driving force for Na$^+$ efflux. In this condition, P2X2aR desensitized more clearly during sustained agonist application (Fig. 4 A). Under repetitive 485-ms voltage-ramp pulses from −80 to +80 mV, delivered twice per second, the inward current activated by the negative portion of the ramp increased with time. This supports the hypothesis that the pore dilates, but this is masked by the larger decrease of the outward current during the positive portion of the ramp (Fig. 4 B). A shift in the reversal potential accompanied by decreasing slope conductance was also observed in cells bathed in medium containing 140 mM NMDG$^+$ and 15 mM Na$^+$, further indicating that removal of bath Na$^+$ does not account for pore dilation (Fig. 4 C).

To remove the influence of oppositely directed Na$^+$ and NMDG$^+$ fluxes on whole cell current during initial agonist application, in further experiments with P2X2aR, the Na$^+$ concentration was made identical in the extracellular and intracellular solutions in the experiments illustrated in Fig. 4 (D–F). In cells bathed in 145 mM NaCl, 10 mM HEPES, and 10 mM glucose, the whole cell recording at a holding potential of +60 mV shows an early development of desensitization in addition to sustained desensitization (Fig. 4 D). Receptor desensitization was also observed in cells bathed in the same medium under a ramp protocol. In contrast to experiments with NMDG$^+$ (Fig. 4 B), a proportional decrease in the inward and outward current amplitudes was observed (Fig. 4 E). Finally, no shifts in reversal potential were observed during 45-s agonist application, but there was a progressive decrease in the slope conductance during sustained agonist application (Fig. 4 F). When cells were bathed in KR buffer, the decay in current was more pronounced during initial and sustained agonist stimulation, indicating faster receptor desensitization under these ionic conditions (Fig. 4 G). Desensitization of P2X2aR was also observed under repetitive 485-ms voltage-ramp pulses delivered twice per second (Fig. 4 H), causing a progressive decrease in the slopes of the I-V curves (Fig. 4 I).

Pore dilation and shift in reversal potential in the model
The paradoxical finding of pore dilation (manifest as a positive shift in reversal potential) together with a
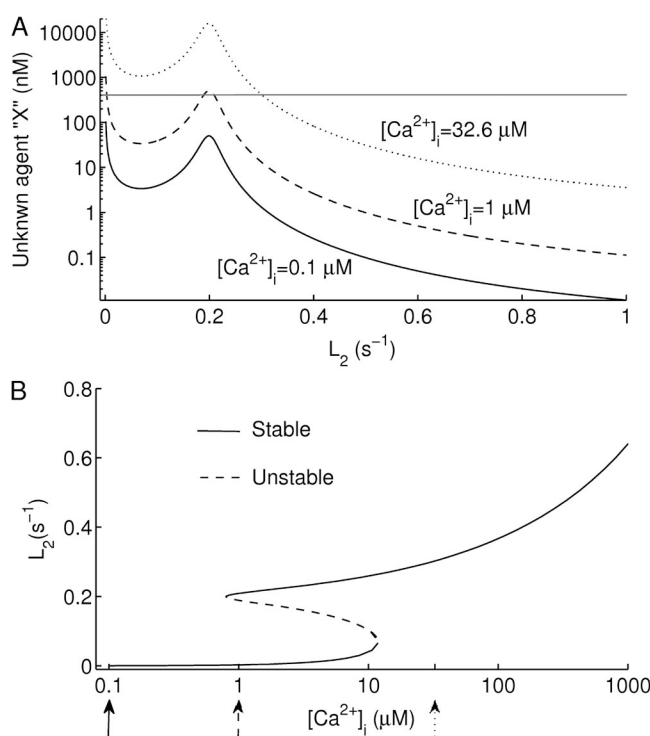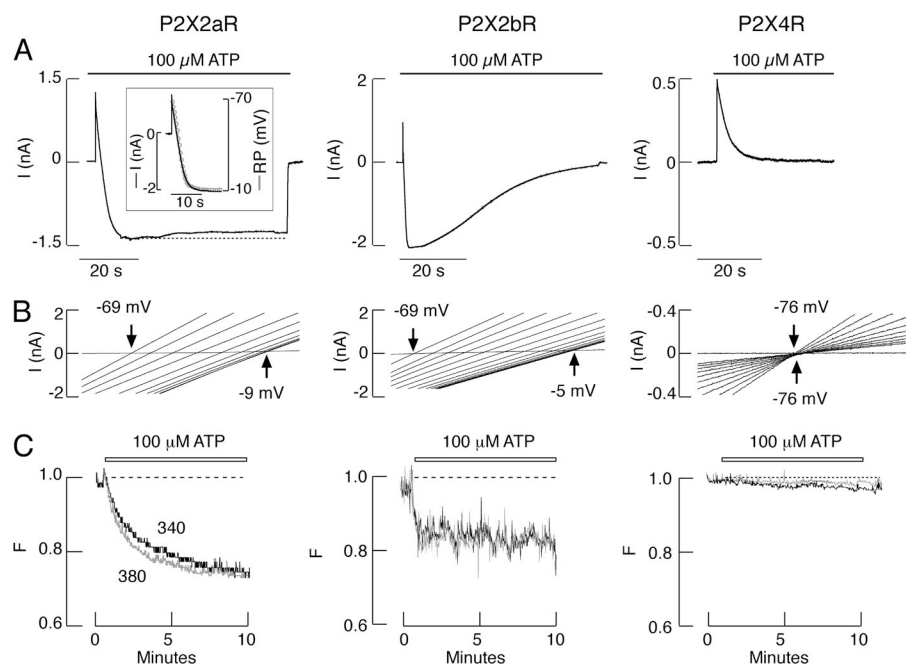
Figure 3. Permeability of recombinant P2X2Rs. Rat P2X2aR, P2X2bR, and P2X4R were expressed in HEK293 (A and B) or GT1 (C) cells, and recording was done in single cells 24 h after transfection using whole cell patch-clamp mode (A and B) or imaging techniques (C), as described in Materials and methods. All experiments were done with naive cells, i.e., during initial agonist application. (A) Patterns of ATP (100 µM)-induced current in HEK293 cells bathed in medium containing 155 mM NMDG$^+$, 10 mM HEPES, and 10 mM glucose only. Currents were recorded at a -60-mV holding potential during 60-s agonist application. Note the lack of inward current in agonist-stimulated P2X4Rs. (Inset) Temporal correlation between P2X2aR current (black) and reversal potential (gray). (B) Positive shifts in reversal potential observed during the initial 25-s agonist application in HEK293 cells bathed in the same medium. In experiments with P2X2aR- and P2X4R-expressing cells, 0.485-s voltage ramps were delivered twice per second from a holding potential of 0 mV (P2X2aR) or -60 mV (P2X4R); 10 out of 50 traces for the I-V relationship with equal time intervals are shown (progressing from left to right). In experiments with P2X2bR, 48.5-ms voltage ramps were delivered twice per 100 ms from a holding potential of 0 mV; the first 15 traces for the I-V relationship with equal time intervals are shown. (C) Effects of ATP on Fura-2 leak in GT1 cells bathed in Ca^{2+}-deficient KR buffer. Normalized fluorescence intensities (gray, $\lambda_{ex} = 380$; black, $\lambda_{ex} = 340$ nm) are shown.

reduction in slope conductance can be reconciled using the kinetic (Markov state) model. We initially considered the case of Fig. 3, in which the medium contained only NMDG$^+$, by excluding the bottom row of Fig. 1 (i.e., the Ca^{2+}-dependent desensitization). To reproduce those experimental recordings, we needed to reduce
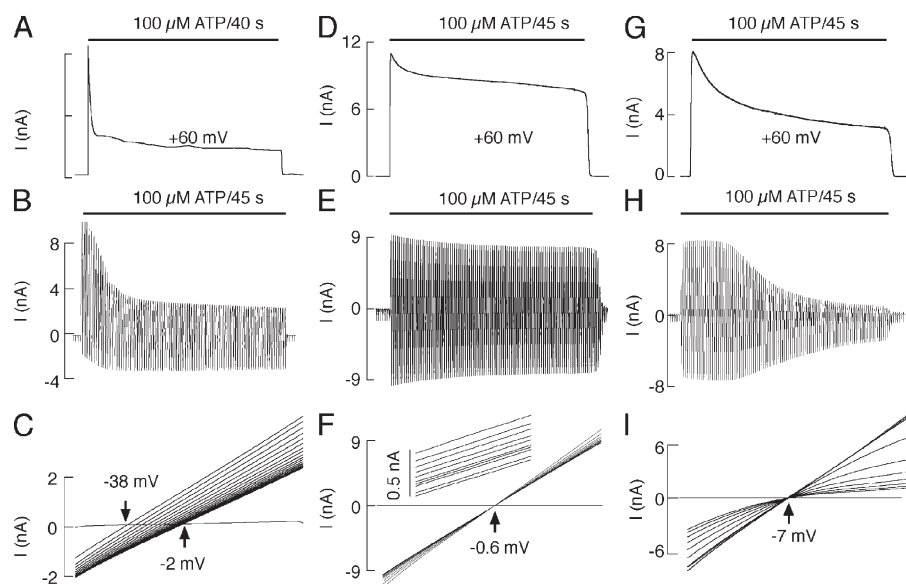

Figure 4. Characterization of P2X2aR pore dilation. All recordings were done in HEK293 cells. (A and B) Patterns of 100 µM ATP-induced current in cells bathed in medium containing 155 mM NMDG$^+$, 10 mM HEPES, and 10 mM glucose. (A) Currents displayed during initial 40-s agonist application at +60 mV. (B) Time course of agonist-induced current under the ramp protocol. (C) Positive shifts in reversal potential observed during the initial 9-s application of 100 µM ATP to a cell bathed in medium containing 140 mM NMDG$^+$, 15 mM NaCl, 10 mM HEPES, and 10 mM glucose. (D–F) Patterns of 100 µM ATP-induced responses when Na$^+$ concentration was identical in the extracellular and intracellular solutions (145 mM). Bath medium also contained 10 mM HEPES and 10 mM glucose. (D) Representative whole cell recording at a holding potential of +60 mV. (E) Time course of agonist-induced current under the ramp protocol. (F) There is no positive shift in reversal potential but a gradual decrease in the slope of current during 45-s agonist application. Shown are 10 ramps spaced by 5 s. (G–I) Patterns of 100 µM ATP-induced responses in cells bathed in KR buffer. (G) Representative whole cell recording at a holding potential of +60 mV. (H) Time course of agonist-induced current under the ramp protocol. (I) The progressive decrease in the slope of current during 45-s agonist application. Shown are 10 ramps spaced by 5 s. In all cases, 485-ms voltage ramps were delivered twice per 1 s from a holding potential of 0 mV (C) and -60 mV (F and I).
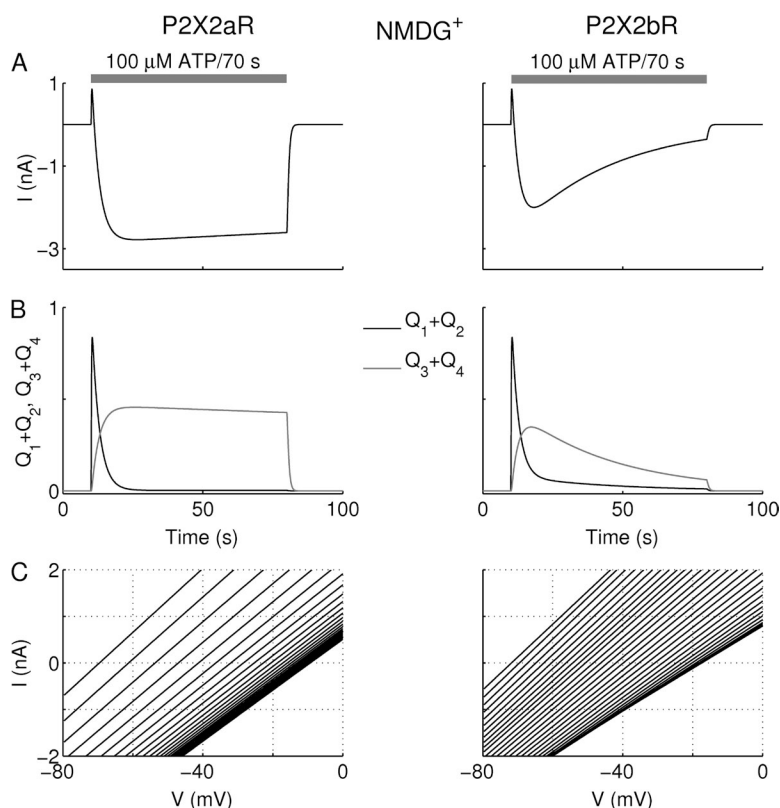
Khadra et al. 339

Figure 5. Simulations of pore dilation using the kinetic model. Pore dilation is manifest as a reversal potential shift (compare Fig. 3). The response of P2X2aR (left) and P2X2bR (right) to 100-µM ATP stimulation for 70 s in the presence of NMDG+-only medium. (A) Current simulations initially exhibiting a brief and small outward current generated by P2X2aR- and P2X2bR-expressing model cells followed by an inward current. The current is outward because states Q_1, Q_2 have reversal potential (E_{12}) more negative than the holding potential V. P2X2aR currents desensitize much more slowly than P2X2bR, because the loss of dilated states is more prominent in the latter. The very fast accumulation of receptors in states $Q_1 + Q_2$ relative to the slow accumulation of receptors in the states $Q_3 + Q_4$ (B) is essential for reproducing the shift in the reversal potential in the I-V curves (C) during voltage ramps (-80 to $+80$ mV delivered twice per second to P2X2aR and twice per 100 ms to P2X2bR). The slopes of the I-V curves in C decrease because $L_3 > L_4$ (i.e., desensitization masks dilation).

the Ca^{2+}-independent desensitization rate (L_3) by 50% for both P2X2aR and P2X2bR versus standard KR buffer (see Table 1). As shown in Fig. 5 A, stimulating P2X2aR (left) and P2X2bR (right) with 100 µM ATP for 70 s initially generated a brief, small-amplitude outward current, because the reversal potential E_{12} of states Q_1 and Q_2 was more negative than the holding potential V.

The ATP concentration was high enough that, after the first few seconds, the receptors shifted beyond the open state Q_2 to the dilated states Q_3 and Q_4, whose reversal potential E_{34} was negative. The time course of dilation was governed by the transition rate $L_4 = 0.3$ and masked by the two transition rates L_3 and L_5 that generate desensitization. This shift produced an inward current in
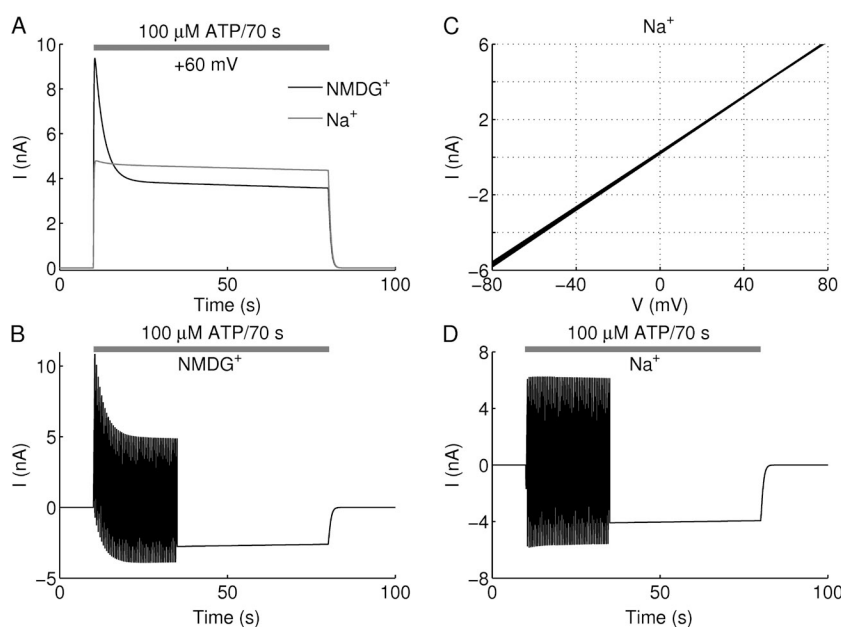

Figure 6. Model illustration of P2X2aR pore dilation with the kinetic model. (A) Current simulations are obtained by stimulating model cells with 100 µM ATP for 70 s under conditions specified by NMDG+ (black)- and Na+ (gray)-containing media. Because the holding potential is +60 mV, an outward current is generated in both cases. The decline in the current with NMDG+ case is steeper than with Na+ because E_{12} is more negative in the former than in the latter. (B) Current simulation obtained during 100-µM ATP stimulation for 70 s and -80 to $+80$ voltage ramps delivered twice per second with parameters corresponding to NMDG+-containing medium. (C) I-V curves generated by the kinetic model during 70-s stimulation with 100 µM ATP and applying -80 to $+80$–mV voltage ramps twice per second in Na+-containing medium. There is little or no shift in reversal potential, but the slopes of the I-V curves decrease. (D) The time course of the current generated using the same conditions described in C. The amplitude of both inward and outward currents declines, resulting in a decrease in the slopes of the I-V curves shown in C.

both types of receptors, but current desensitization was faster for P2X2bR than for P2X2aR, in agreement with Fig. 3; this was achieved by making L_5 larger for P2X2bR (Table 1).

Fig. 5 B shows that, for the first 15 s of ATP stimulation, receptor accumulation and decline in $Q_3 + Q_4$ (gray) is much slower than in $Q_1 + Q_2$ (black). In the -80 to $+80$–mV voltage-ramp simulations done in Fig. 5 C, this feature was crucial for both receptors to exhibit (a) a shift in reversal potential from -69 mV to the steady-state value of -10 mV, as found in the experimental I-V curves (Fig. 4 C), and (b) a progressive decrease in their slopes indicating a decline in conductance. The model suggests that the slopes of the I-V curves became shallower because dilation was masked by Ca^{2+}-independent desensitization. In terms of the scheme in Fig. 1, receptors transition from Q_2 to Q_3, which has a more positive reversal potential and a larger single-channel conductance, but at the same time receptors are lost from Q_2 to the desensitized state D_4. Because almost all of the receptors that are open are in state Q_3, after the first few seconds, the whole cell reversal potential is shifted in the positive direction, but the number of open channels and the total cell conductance decrease from their peak values (see the supplemental text for a quantitative analysis of this outcome).

The kinetic model of P2X2aR was able to account as well for the results in Fig. 4 (A–F), in which the medium contained either $NMDG^+$ or Na^+ and the holding potential was $+60$ mV. As before, the bottom row of Fig. 1 was excluded, and the Ca^{2+}-independent desensitization (L_3) was made slower than the case for standard KR buffer (50% reduction for $NMDG^+$ and 75% reduction for Na^+). Fig. 6 A shows outward currents with the same characteristics as in the experimental recordings in Fig. 4 (A and D) during 70-s stimulation with 100 µM ATP. As in the experiments, a small degree of Ca^{2+}-independent desensitization was observed in both cases, with a larger peak current in the $NMDG^+$ case (Fig. 6 A, black), because E_{12} is assumed to be more negative for $NMDG^+$ than for Na^+ (gray).

Fig. 6 B shows simulated currents produced by ramps from -80 to $+80$ mV delivered twice per second. In agreement with the experiments in Fig. 4 B with $NMDG^+$-containing medium, the model currents exhibited a sharp decline in the outward current and a lesser increase in the inward current. The inward current is carried mainly by the dilated receptors, because it is generated in the early part of the ramp when the driving force for the nondilated current is small. Its growth is caused by dilation (the growth of $Q_3 + Q_4$; see Fig. 5 B). The outward current is initially carried mainly by the nondilated open receptors, $Q_1 + Q_2$, but eventually by the dilated receptors, $Q_3 + Q_4$. The decrease in the outward current is caused by the desensitization of the nondilated receptors in state Q_2, which exceeds the growth

of the dilated receptors. Thus, it is just another manifestation of the masking of dilation by desensitization discussed in the context of Fig. 5.

Repeating the same simulations in medium containing Na^+ but not $NMDG^+$ (as in the experiments in Fig. 4 E), the kinetic model also generated I-V curves with no (or insignificant) shift in reversal potential centered around 0 mV (as shown in Fig. 6 C), and simulated current exhibited a slight decline in inward and outward currents during first 15 s of voltage-ramp applications (as shown in Fig. 6 D). The agreement between the model and the data in media both containing only $NMDG^+$ and only Na^+ supports the hypothesis that the transition from Q_2 to Q_3 for P2X2R, representing dilation, is slow and that the channel first opens then dilates, but dilation is masked by desensitization.

Time course and ATP concentration dependence of P2X2R activation and desensitization

In further experiments, P2X2aR and P2X2bR were bathed in normal KR buffer and stimulated with 100 µM ATP several times for 45 s, followed by a 4–5-min washout period. Current was recorded in cells at a holding
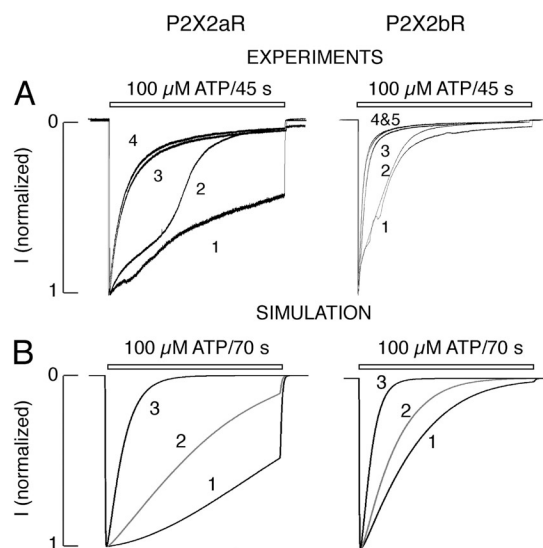

Figure 7. Time course of P2X2R desensitization: experiments and simulations. (A) Patterns of current responses during repetitive agonist application in HEK293 cells bathed in KR buffer. P2X2aR I_{max}: 3.5 (1), 3.5 (2), 3 (3), and 3.2 (4) nA; P2X2bR I_{max}: 6.6 (1), 6.5 (2), 6.5 (3), 5 (4), and 4.5 (5) nA. (B) Current simulations (normalized by their maximum amplitudes) obtained using the kinetic model (and default values in Table 1). Currents are generated by repetitively stimulating model cells expressing P2X2aR (left) and P2X2bR (right) three times with 100 µM ATP for 70 s with a washout period of 250 s. P2X2aR I_{max}: 3.5 (1–3) nA; P2X2bR I_{max}: 3 (1–3) nA. Repetitive stimulation of both receptors increased desensitization at each consecutive pulse as a result of calcium entry and activation of Ca^{2+}-dependent desensitization (i.e., a shift to the bottom row of Fig. 1). The simulations suggest that receptor desensitization is more expressed in P2X2bR as a result of the dominance of L_5 in these receptors.

potential of −60 mV. Fig. 7 A shows responses of HEK293 cells bathed in KR buffer. P2X2aR responded to the initial application of agonist with a rapid rise in current, followed by gradual decline of current, reaching ∼50% of the peak of current amplitude at the end of agonist application. P2X2bR desensitization during initial agonist application was faster than that of P2X2aR. The receptor-specific pattern of desensitization was also observed in cells bathed in medium in which bath Na^+ was replaced with $NMDG^+$ and held at +60 mV (Fig. 3 A) and −60 mV (Fig. S1). With both P2X2aR and P2X2bR expressed in HEK293 cells, the rate of desensitization markedly increased during the course of the subsequent agonist application (Fig. 7 A). We termed facilitation of receptor desensitization during repetitive agonist application "use-dependent desensitization."

The toggle switch character of the Ca^{2+}-dependent desensitization rate L_2 (Fig. 2) is needed to explain use-dependent desensitization. A rise in $[Ca^{2+}]_i$ caused by calcium entry into the cell during ATP stimulation would initially lead to a gradual increase in the value of L_2. If $[Ca^{2+}]_i$ surpasses the right knee of the S-shaped curve, however, L_2 would jump to a high steady-state level, inducing a rapid increase in the desensitization rate (Fig. S2). If ATP stimulation is maintained, and $[Ca^{2+}]_i$ continues to increase, the desensitization rate continues to rise as well. When ATP is removed during washout periods, $[Ca^{2+}]_i$ decreases slowly and may remain higher than the level of the left knee. If so, L_2 would remain elevated at the next ATP application.

In Fig. 7 B, we simulated the experiments of Fig. 7 A done in HEK293 cells. Currents, normalized by their maximum amplitudes, were plotted after stimulating model cells, representing either P2X2aR (Fig. 7 B, left) or P2X2bR (right), repetitively three times with 100 μM ATP for 70 s, interrupted with 250-s washout periods; the model now includes all the states in Fig. 1 without excluding any row. At each pulse, an inward current with fast activation was generated, and the desensitization was enhanced with each consecutive pulse. (No outward currents were obtained here because the assumed reversal potentials of Q_i, i = 1,2,3,4, were less negative than the holding potential, in contrast to the previous simulations in which $NMDG^+$ was the only cation in the medium.) The activation phase was fast because the forward rates in each row were large (see Table 1). The changes in current amplitudes from pulse to pulse (not depicted) were very small and comparable to those obtained experimentally.

Of note in Fig. 7 A, a dramatic increase in desensitization rate between the second and third ATP pulses was exhibited by both P2X2aR and P2X2bR. The model captures this behavior (Fig. 7 B) via a jump in the value of L_2 from the bottom to the top branch of the S-curve in Fig. 2 B, caused by Ca^{2+} entry through the channels. ATP washout led to receptor deactivation and the return

of current amplitudes to basal level, but desensitization did not reset to its basal level because L_2 remained on the upper branch of the S-curve; with a longer washout period, L_2 would eventually return to its basal level.

To exclude the possible contribution of P2YRs expressed endogenously in HEK293 cells on P2X2R gating, we also used GT1 cells. Under the ionic conditions listed above, both receptor types showed patterns of activation and desensitization highly comparable to those observed in HEK293 cells, and repetitive agonist application was accompanied by increased rates of receptor desensitization (Fig. 8 A).

To exclude the possible impact of whole cell recording on gating, intact cells were loaded with Fura-FF dye, which has lower sensitivity for Ca^{2+} than for Fura-2, and were bathed in KR buffer and stimulated with 100 μM ATP. In cells with larger Ca^{2+} influx, this dye permits good estimates of the peak amplitude of signals, a feature critical in clarifying the pattern of early response, but gives unreliable estimates when Ca^{2+} influx is low. Fig. 8 B shows that both receptors generated a rapid rise in $[Ca^{2+}]_i$ but exhibited different rates of desensitization.

To study the concentration dependence of P2X2aR and P2X2bR activation and desensitization, only records obtained during the third agonist application were used for analysis (Fig. 9 A). In all ATP concentrations, the
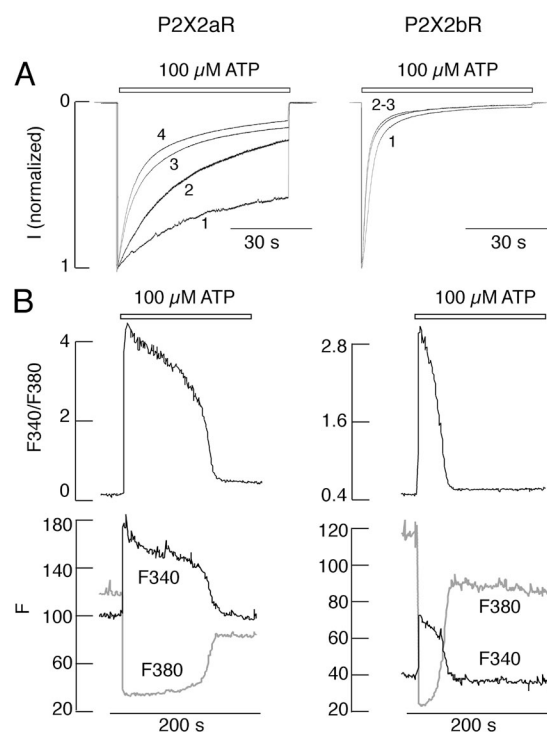

Figure 8. ATP-induced inward current and calcium responses in GT1 cells bathed in KR buffer. (A) Repetitive stimulation of cells clamped at −60 mV. P2X2aR I_{max}: 4.5 (1), 3.5 (2), 3.1 (3), and 3.1 (4) nA. P2X2bR I_{max}: 5.1 (1), 3.2 (2), and 3.1 (3) nA, from bottom to top. (B) ATP-induced changes in $[Ca^{2+}]_i$ during initial agonist application, as reported by fluorescence ratio of Fura-FF.

best approximation for decay of current during sustained application was achieved with monoexponential fits, and the calculated time constants (τ) are shown above the traces (Fig. 9 A). The concentration dependence of the peak current responses of P2X2aR and P2X2bR on ATP is shown in Fig. 9 B, and the dependence of the level of receptor desensitization for 40-s application on agonist concentration is shown in Fig. 9 C. The EC_{50} values for receptor desensitization were comparable to the corresponding values for receptor activation. These experiments indicate that the rates of P2X2aR and P2X2bR activation and desensitization were determined by agonist concentration; the two splice forms of P2X2R do not differ in sensitivity to ATP, and P2X2bR desensitizes more rapidly, especially at higher agonist concentrations. In further experiments, cells were always stimulated with 100 µM ATP, a level at which the rates of desensitization of the two receptor subtypes were markedly different.

Model simulations of dependence of current simulations (normalized by their maximum amplitude) and receptor accumulation in open states on ATP concentration during third application are shown in Fig. 10. The relationship between L_2 and ATP concentration is summarized in Fig. S3. In agreement with the experimental data, current simulations of Fig. 10 A show that the desensitization phase of both P2X2aR (left) and P2X2bR (right) increased with increasing the ATP dose (using the concentrations 1, 3.2, 10, 32, and 100 µM).

More rapid desensitization of P2X2bR compared with P2X2aR at each dose was achieved by making L_5 larger. Such outcomes can be understood by examining receptor accumulation in open states shown in Fig. 10 B for both P2X2aR (left) and P2X2bR (right). At low ATP concentration (≤ 3.2 µM), only a small fraction of receptors reached $Q_1 + Q_2$ (Fig. 10 B, black), and almost none reached $Q_3 + Q_4$ (gray). Increasing the concentration of ATP stimulation, however, led to a gradual increase in the fraction of receptors reaching $Q_1 + Q_2$ and $Q_3 + Q_4$, increasing the proportion of receptors exposed to Ca^{2+}-dependent desensitization via L_2 (Fig. 1) and thus the degree of current desensitization.

Dependence of P2X2R gating on calcium

Comparison of the rates of P2X2a receptor desensitization in cells bathed in $NMDG^+$ or Na^+-containing medium (Figs. 3 and 4), with the rates in KR medium (Figs. 7–9), suggests that the rates of receptor desensitization in whole cell recording depend on bath Ca^{2+}. To clarify this issue, we varied bath and intrapipette calcium concentrations as indicated in Fig. 11. When Ca^{2+} was not added to KR buffer and the residual Ca^{2+} was buffered by the addition of 0.5 mM EGTA, only marginal receptor desensitization was observed during 45-s application of 100 µM ATP, and only a small change in the rate of receptor desensitization occurred during repetitive agonist application (Fig. 11 A). In cells bathed in Ca^{2+}-deficient medium without EGTA, the rate of receptor
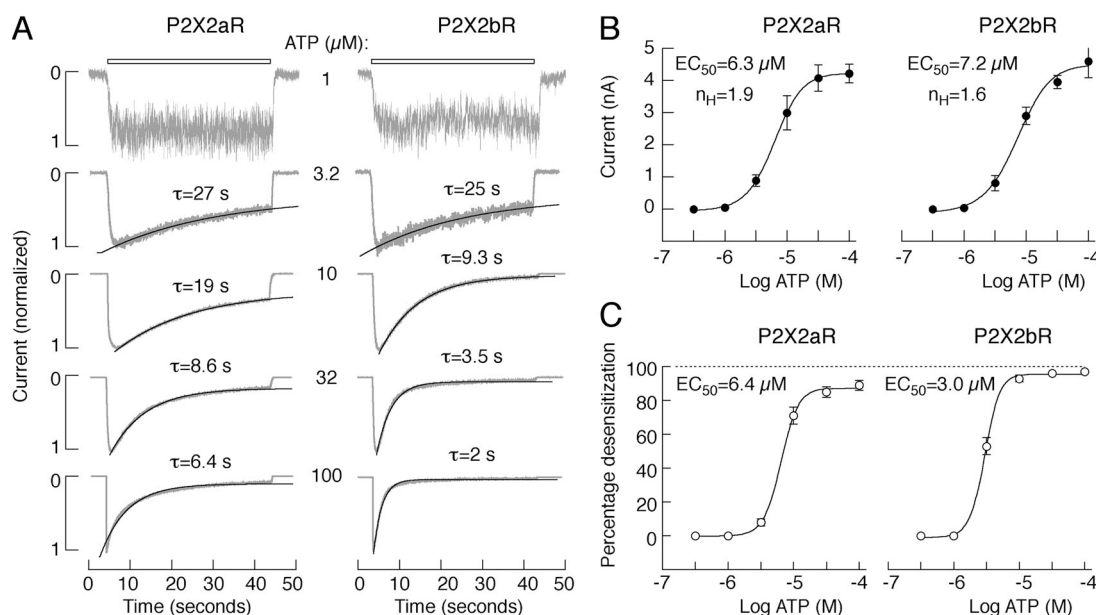

Figure 9. Concentration-dependent effects of ATP on activation and desensitization of inward current in HEK293 cells expressing P2X2aR and P2X2bR whole cell recording. (A) Typical pattern of P2X2aR (left) and P2X2bR (right) currents in response to variable ATP concentrations. Traces shown are obtained during the third application of ATP. Gray lines, experimental traces; black lines, fitted curves. τ is from monoexponential fitting. (B) Dependence of the peak current amplitude on agonist concentration in cells expressing P2X2aR (left) and P2X2bR (right). (C) Dependence of the level of receptor desensitization on agonist concentration in cells expressing P2X2aR (left) and P2X2bR (right). In A, representative traces are shown; in B and C, mean ± SEM values from at least four recordings per dose are shown.

desensitization was faster and further increased during repetitive agonist application (Fig. 11 B). When the receptor was activated in bath medium containing 2 mM Ca^{2+}, a rapid and almost complete desensitization occurred during the initial agonist application. Subsequent receptor stimulation caused further increase in the rate of desensitization (Fig. 11 C). After the third agonist application, P2X2aR desensitized rapidly, with a rate similar to the rates of rapidly desensitizing P2X1R and P2X3R (North, 2002). These results indicate that under whole cell recording, Ca^{2+} influx plays an important role in use dependence of desensitization.

In further experiments, we compared the pattern of P2X2aR desensitization using three different current recording configurations in HEK293 cells: whole cell, outside-out macropatch, and perforated cells. A typical example of the whole cell current achieved during the

second application of 100 µM ATP in cells bathed in KR buffer and with pipette containing 145 mM NaCl, 10 mM EGTA, and 10 mM HEPES is shown in Fig. 11 D. At the end of stimulation, the outside-out macropatch mode was achieved by pulling the pipette away from the cell, and 100 µM ATP was again applied. Under such experimental conditions, the receptor activated and desensitized rapidly. In the second experiment, cells were bathed in KR buffer, and membrane perforation was achieved by amphotericin. In perforated cell recording mode, repetitive agonist application did not change current responses much, with rates of desensitization highly comparable to those observed in the whole cell recording during third agonist application (Fig. 7 A). When cells were bathed in Ca^{2+}-deficient KR buffer, the rate of P2X2aR was slow (Fig. 11 E, inset) and highly comparable to that observed in the whole cell recording
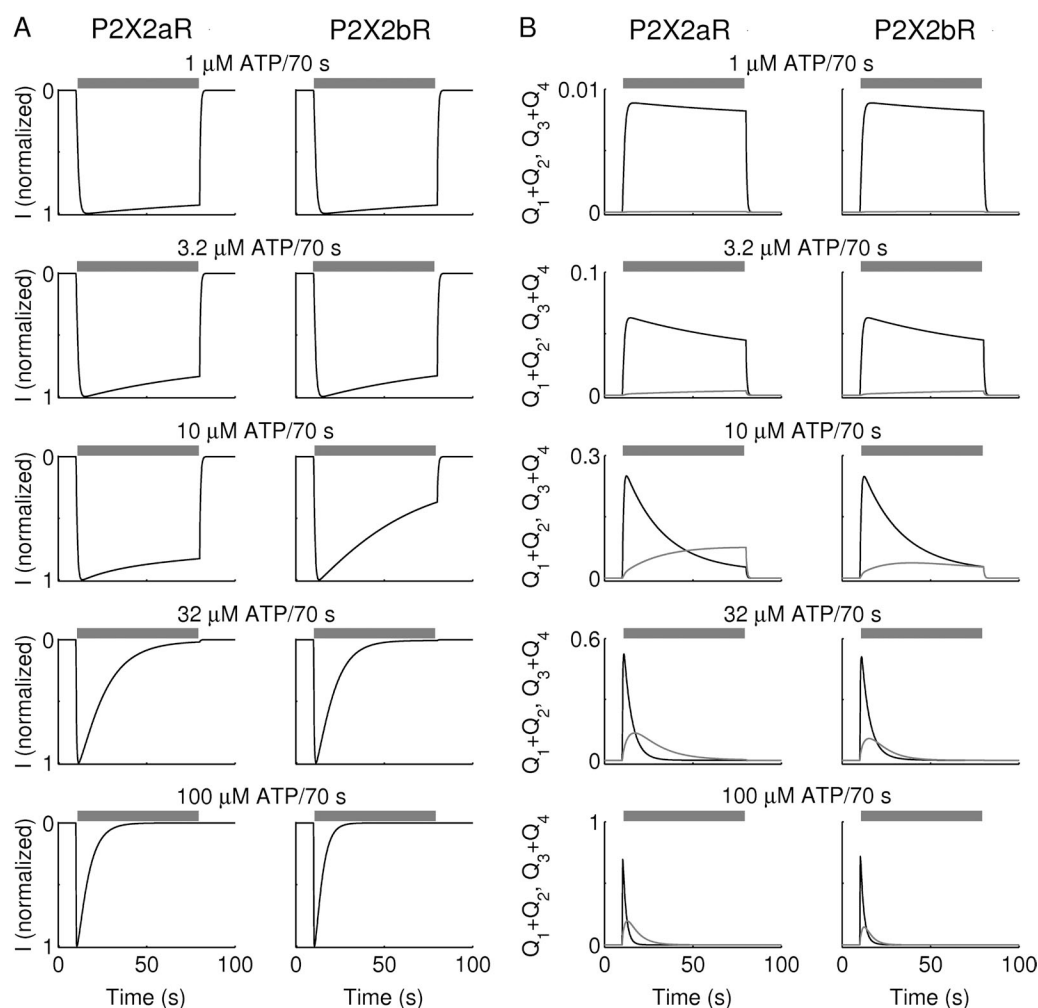

Figure 10. Dependence of current amplitude and desensitization of P2X2aR and P2X2bR on ATP concentration in the kinetic model. (A) Simulated currents normalized by their maximum amplitudes, and (B) receptor accumulation in $Q_1 + Q_2$ (black) and $Q_3 + Q_4$ (gray), obtained during the third stimulation of P2X2aR (left) and P2X2bR (right) with 1, 3.2, 10, 32, and 100 µM ATP for 70 s, as indicated by the gray bars (washout periods are 250 s). Increasing ATP dose increases receptor accumulation in $Q_3 + Q_4$, which in turn activates the Ca^{2+}-dependent desensitization via the state Q_3, leading to an increase in current desensitization in both receptors. Because L_5 is smaller for P2X2aR, simulated P2X2b currents desensitize faster than P2X2a currents, in agreement with experimental observations (Fig. 9).

when cells were bathed in Ca^{2+}-deficient KR buffer supplemented with 0.5 mM EGTA (Fig. 11 A) and Ca^{2+}-deficient/$NMDG^+$-containing medium (Fig. 3 A). We conclude that Ca^{2+}-dependent P2X2R desensitization is a native characteristic of P2X2R, whereas the use dependence of desensitization could reflect altered Ca^{2+} handling in the whole cell recording or dialysis of some intracellular messenger factor.

The kinetic model representing P2X2aR-exressing cells was also successful in capturing the effects of the various extracellular Ca^{2+} and buffer concentrations and experimental conditions used in Fig. 11. As before, the model cells were repetitively stimulated with 100 µM ATP for 70 s, with washout periods of 250 s, and current simulations (normalized by their maximum amplitude) were recorded. We modeled the effects of various levels of $[Ca^{2+}]_e$ and buffer concentration (Fig. 12) by increasing the value of f, the fraction of free Ca^{2+} in the medium, from 0 (A) to 0.005 (B) and to 0.05 (C). In the first case, four repetitive stimulations produced current simulations that overlaid each other and exhibited no increase in the desensitization rate L_2, because the bottom row of Fig. 1 was never reached. Increasing f to 0.005 in Fig. 12 D allowed $[Ca^{2+}]_i$ to rise higher and led to an increase in the value of L_2 at each consecutive pulse, resulting in more transitions to the bottom row. There was, however, no significant jump in the value of L_2 because the increase in $[Ca^{2+}]_i$ was insufficient to cross the right knee of Fig. 2 B. Finally, when f was increased to 0.05, Ca^{2+} entry into the cell during the very first ATP stimulation was large enough to cross the right knee and induce L_2 to jump to the upper stable branch of the S-curve of Fig. 2 B, generating a very fast desensitization phase. Follow-up ATP stimulations led to further

increases in L_2 along the upper branch of the toggle switch as a result of a further increase in $[Ca^{2+}]_i$.

Fig. 7 A showed that desensitization not only became more rapid with successive stimulation but also could become more rapid during the course of a single agonist application (shown, for example, during the second ATP application in Fig. 7 A). This "wiggling" is caused by a jump in the value of L_2 from the lower branch of the S-shaped toggle switch to the upper branch during the course of ATP stimulation. The model captured this wiggling behavior (Fig. 12 D) during the second simulation (gray) when the P2X2aR-expressing model cell was repetitively stimulated with 100 µM ATP for 70 s. This behavior was achieved by increasing the parameter $\beta_1 = 130 \text{ s}^{-2} \cdot \text{M}^{-1}$, in Eq. 17, making L_2 more sensitive to $[Ca^{2+}]_i$ and moving the knees of the S-shaped curve in Fig. 2 B to the left (see Fig. S4 A, right). Simulations suggest that variability in this feature could be partially responsible for the heterogeneity observed in experimental recordings.

Finally, in Fig. 12 E, we compared the whole cell recording (black) to the outside-out recording (gray) by adjusting the value of f according to each configuration. By increasing the value of f from 0.01 in the whole cell configuration to 0.03 in the outside-out configuration, to reflect the smaller volume of the macropatch compared with the cell, we were successful in capturing the more rapid desensitization in the outside-out case (Fig. 12 E, left). This outcome was a consequence of the more rapid accumulation of free calcium in the cytosol (Fig. 12 E, right) in the latter simulations than in the former and thus generating a higher rate of transitions to the Ca^{2+}-dependent desensitization states (bottom row of Fig. 1).
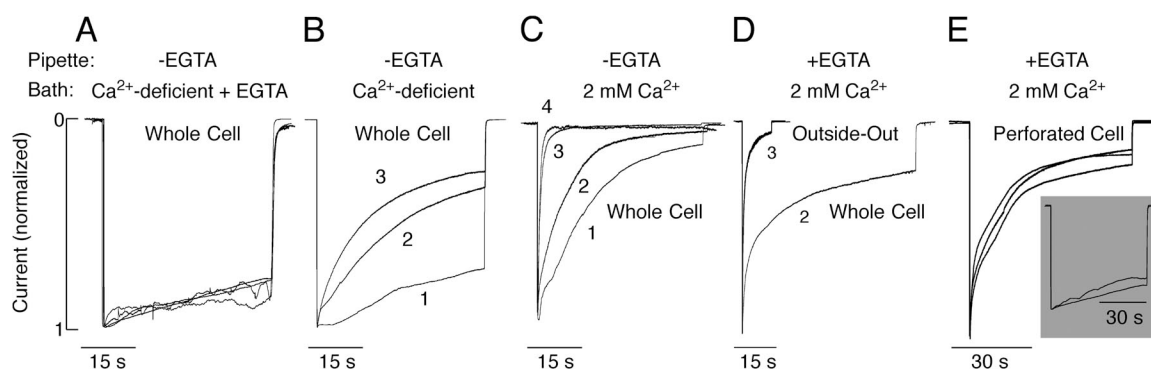

Figure 11. Dependence of P2X2aR desensitization kinetics on bath and intrapipette Ca^{2+} concentration. All experiments were performed in HEK293 cells. (A–C) Effects of variable bath Ca^{2+} concentrations on P2X2aR desensitization. Cells were bathed in Ca^{2+}-deficient KR buffer containing 0.5 mM EGTA (A), Ca^{2+}-deficient KR buffer (B), and 2 mM of Ca^{2+}-containing buffer (C). In all these experiments, the intrapipette buffer did not contain EGTA. I_{max}: 4.6 (1), 4.5 (2), 4.5 (3), and 4.1 (4) nA (A); 3.5 (1), 3.5 (2), and 3.2 (3) nA (B); and 5.5 (1), 2.6 (2), 2.2 (3), and 2.2 (4) nA (C). (D and E) Dependence of the rate of P2X2aR desensitization on the mode of recording. Cells were bathed in KR buffer and stimulated with 100 µM ATP. (D) Whole cell (second agonist application, I_{peak} = 4.5 nA) versus outside-out macropatch (third agonist application, I_{peak} = 0.4 nA) recording. (E) Perforated cell recording. (Main panel) Cells were bathed in 2 mM of Ca^{2+}-containing KR. I_{peak} = 4.7 (1), 2.6 (2), and 2.3 (3) nA. (Inset) Cells were bathed in Ca^{2+}-deficient KR medium.

DISCUSSION

The main goal of our study was to investigate the permeability and conductance of P2X2aR and P2X2bR during sustained and repetitive agonist application. These receptors are permeable to monovalent and divalent cations but also show a time-dependent increase in P_{NMDG}/P_{Na} that is commonly used as a mark of entry into the dilated state (Egan et al., 2006). Here, we showed that the change in P_{NMDG}/P_{Na} is faster for P2X2aR (within 10 s) than previously measured for P2X7R (within 20–30 s) (Yan et al., 2008), which is consistent with the P2X2R literature (Eickhorst et al., 2002; Fisher et al., 2004). As with P2X7R (Yan et al., 2008), we also observed leak of Fura-2 in P2X2R-expressing cells. Under the same experimental conditions, only a marginal shift in the reversal potential and no leak of Fura-2 was observed in P2X4R-expressing cells, further suggesting that the P2X2R recordings are not experimental artifacts. Movement of the P2X2aR C-terminal domain measured by fluorescence resonance energy transfer occurs with a comparable time course to the increase in P_{NMDG}/P_{Na} (Fisher et al., 2004). This is consistent with observations about the relevance of this part of the receptor molecule for regulating the ionic permeability to larger organic cations (Chaumont et al., 2004; Khakh and Egan, 2005). Here, we showed that deletion of 69 residues in the C terminal of P2X2bR does not eliminate conductivity for larger organic cations but changes the time course.

It is generally accepted that the time-dependent transition from open to dilated state in P2X7R is accompanied by the development of I_2 (Egan et al., 2006). However, in none of the experimental conditions (whole cell and perforated patch-clamp recordings, repetitive agonist applications of variable durations, concentration-dependent studies, and/or different ion conditions) were we able to observe the presence of I_2 in P2X2R-expressing cells. Furthermore, although there was a progressive shift in the reversal potential in experiments with $NMDG^+$ in the bath solution and Na^+ in pipette solution, we (Figs. 3 and 4) and others (Fisher et al., 2004; Chaumont and Khakh, 2008) observed that the slopes of I-V curves decreased, in contrast to activated P2X7R (Yan et al., 2008). Our experiments and model provide a plausible explanation for this phenomenon. The total conductance decreases as a result of rapid and Ca^{2+}-independent desensitization of the naive receptors while at the same time the proportion of conductance carried by the dilated states increases, so the reversal potential moves toward that of the dilated receptors. The total conductance shrinks, but the dilated receptors account for more of it. The failure to observe I_2 is explained by the fact that dilation is masked by simultaneous desensitization.

As was well established in previous studies, P2X2bR desensitizes more rapidly than P2X2aR, reflecting the lack of 69 residues in its C terminal (Brändle et al., 1997; Simon et al., 1997; Koshimizu et al., 1998b, 2006;
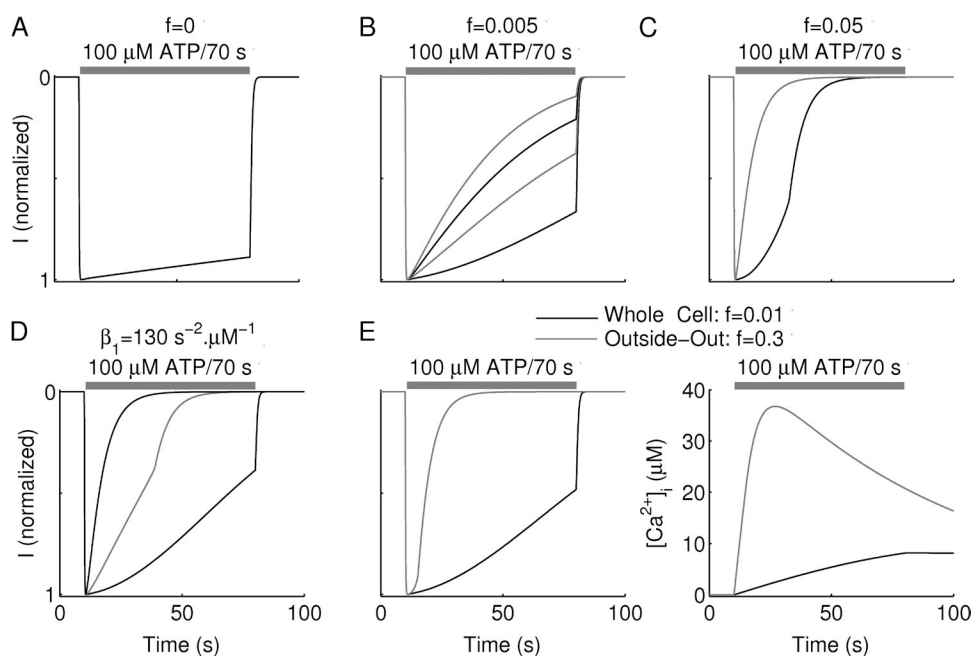

Figure 12. Simulations of use dependence of desensitization based on the kinetic model for P2X2aR. Currents correspond to stimulations with 100 µM ATP for 70 s, as indicated by the gray bar, in the presence of various $[Ca^{2+}]_e$ and were normalized by their maximum amplitudes (I_{max} is 3.5 nA in all of these simulations, and washout period is 250 s). (A–C) Repetitive stimulation at variable $[Ca^{2+}]_e$ modeled by varying the fraction of free Ca^{2+}, f. Current simulations obtained by setting (A) $f = 0$ to represent Ca^{2+}-deficient medium plus EGTA (the four traces overlie each other, indicating that desensitization did not increase because of the loss of Ca^{2+}-dependent desensitization); (B) $f = 0.005$ to represent Ca^{2+}-deficient medium but no EGTA; and (E) $f = 0.05$ to represent 2 mM $[Ca^{2+}]_e$; panels correspond to Fig. 11 (A–C), respectively. (D) Receptor desensitization of P2X2aR changes from slow to fast during the course of the second ATP stimulation (gray line) because of activation of the toggle switch (see Fig. 2 and Results for details); β_1 increased to 130 $s^{-2} \cdot \mu M^{-1}$. (E) Normalized current (left) and $[Ca^{2+}]_i$ (right) simulations in the whole cell (black) and outside-out (gray) configuration. The two configurations were established by setting $f = 0$ for the former and $f = 0.3$ for the latter. Calcium entry and accumulation inside the cell in the whole cell configuration are slower than in the outside-out configuration.

Parker et al., 1998; Housley et al., 1999; Lynch et al., 1999). Earlier studies uncovered the relevance of removal of the Arg^{371}-Pro^{376}–terminal sequence in establishing the P2X2bR-specific pattern of desensitization (Koshimizu et al., 1998a, 1999). Here, we showed that this receptor-specific pattern of desensitization was more obvious when cells were stimulated with higher agonist concentrations. The kinetic model proposed here provides a rationale for this experimental observation. At low agonist concentrations, channels are predominantly in the open state, and their transition from open to desensitized state is roughly the same for both receptors. At higher agonist concentrations, however, a substantial fraction of channels is in the dilated state, which permits faster transitions back to the lower conductance open state and to the Ca^{2+}-independent desensitized states in the P2X2bR case.

Several lines of evidence obtained in experiments with whole cell recording also support the conclusion that both P2X2aR and P2X2bR exhibit Ca^{2+}-dependent desensitization. When Ca^{2+} was not present in KR buffer, and the residual Ca^{2+} was buffered by EGTA, desensitization of P2X2aR was practically abolished. P2X2aR desensitization was also minimal in cells bathed in $NMDG^+$/HEPES/glucose buffer with the pipette containing EGTA, and the rate of P2X2bR desensitization was slower, both compared with cells bathed in KR buffer. When Ca^{2+} was added to $NMDG^+$ bath medium, both receptors desensitized. Desensitization was facilitated in cells bathed in Ca^{2+}-containing KR medium without EGTA in the pipette. In macropatch recording, which facilitates increase in $[Ca^{2+}]_i$ caused by reduced intracellular volume, desensitization was further facilitated.

We also showed that Ca^{2+}-dependent P2X2R desensitization does not depend on the mode of recording, in contrast to the use dependence of desensitization observed only in whole cell recording. These experiments are in general agreement with some experiments performed by others (Ding and Sachs, 2000), indicating that (a) Ca^{2+}-dependent desensitization is a native characteristic of P2X2aR and P2X2bR; (b) the difference in whole cell versus perforated cell mode could indicate the relevance of some intracellular messenger in this process or that intracellular Ca^{2+} handling by cells differs in these experimental conditions; and (c) whole cell recording provides comparable data to perforated patch-clamp recording when cells were bathed in KR buffer with the pipette medium containing 10 mM EGTA, and after the rates of receptor desensitization stabilize during repetitive agonist application.

With the use of a toggle switch (Tyson et al., 2003) to describe the dependence of the desensitization rate L_2 on $[Ca^{2+}]_i$ and exhibiting hysteresis, we were able to model the effects of Ca^{2+} on P2X2R. According to this phenomenological toggle switch model, L_2 is on the lower branch of the switch at low $[Ca^{2+}]_i$ and on the upper branch at high $[Ca^{2+}]_i$. The sharp increase in L_2, once $[Ca^{2+}]_i$ exceeds the right knee of the switch, mediates a change from slow to fast desensitization of the whole cell current. The rapidity of the change is attested by the observation in some cases that the change in the rate of desensitization can occur during a single ATP presentation (Figs. 7 A, experiment, and 12 D, model). The model also demonstrated how the separation of the jump-down point (left knee of the switch) from the jump-up point (right knee) could account for the preservation of fast desensitization during extended periods of washouts, when Ca^{2+} would leave the cell. A more conventional model with a sigmoidal increase in desensitization rate with $[Ca^{2+}]_i$ would not be able to capture this memory effect. The switch model predicts the existence of an L_2-inhibiting factor, which we labeled X. Further studies are needed to identify this factor, which could be a metabotropic mode of regulation of receptor desensitization by some Ca^{2+}-activated pathway, or the relevance of other intracellular messengers in this process.

The behavior of the kinetic model as a whole was fairly robust toward parameter perturbations when certain key parameters were considered. Table S1 illustrates briefly how the features obtained during repetitive stimulation are affected by changes in the values of some key parameters, and Fig. S4 displays the effect of parameter variations on the toggle switch, which conveys the robustness of the S-shaped curve toward these changes. Thus, the model predicts with high confidence that such an S-shaped curve is needed to explain the Ca^{2+} dependence of desensitization, but we cannot determine the mechanism that generates the S-shaped curve without further experimentation. Without this prediction, however, there would be no reason to search for such a mechanism. Our primary modeling goal was to develop a plausible model structure that was compatible with the data, which was a highly challenging task requiring several iterations. In the future it would be desirable to conduct a more systematic sensitivity analysis and exploration of parameter space to determine whether other model structures and parameter sets exist that can account as well or better for the diverse behaviors of P2X2 receptors.

In summary, our results demonstrate that pore dilation is not a unique feature of P2X7R but also occurs in P2X2R-expressing cells, in contrast to P2X4R, which does not dilate when expressed in HEK293 cells. Development of conductivity to $NMDG^+$ occurs in the presence of carbenoxolone, a blocker of pannexin and connexin channels. Our experiments and modeling provide a rationale for the lack of sustained current growth in dilating P2X2Rs. Whereas P2X7R does not desensitize, P2X2R does, and this Ca^{2+}-independent desensitization is enhanced by deletion of 69 residues in the C terminal. The opposing effects of dilation and

desensitization determine the total conductivity, resulting in generation of monophasic P2X2R currents. The receptor desensitization is facilitated in the presence of bath Ca^{2+}, reflecting transition from dilated to desensitized state. Further studies are needed to identify the mechanism of Ca^{2+}-dependent desensitization (allosteric vs. metabolic) and the residues responsible for this process.

REFERENCES

Brändle, U., P. Spielmanns, R. Osteroth, J. Sim, A. Surprenant, G. Buell, J.P. Ruppersberg, P.K. Plinkert, H.P. Zenner, and E. Glowatzki. 1997. Desensitization of the P2X(2) receptor controlled by alternative splicing. *FEBS Lett.* 404:294–298. http://dx.doi.org/10.1016/S0014-5793(97)00128-2

Chaumont, S., and B.S. Khakh. 2008. Patch-clamp coordinated spectroscopy shows P2X2 receptor permeability dynamics require cytosolic domain rearrangements but not Panx-1 channels. *Proc. Natl. Acad. Sci. USA.* 105:12063–12068. http://dx.doi.org/10.1073/pnas.0803008105

Chaumont, S., L.H. Jiang, A. Penna, R.A. North, and F. Rassendren. 2004. Identification of a trafficking motif involved in the stabilization and polarization of P2X receptors. *J. Biol. Chem.* 279:29628–29638.

Coddou, C., Z. Yan, T. Obsil, J.P. Huidobro-Toro, and S.S. Stojilkovic. 2011. Activation and regulation of purinergic P2X receptor channels. *Pharmacol. Rev.* 63:641–683. http://dx.doi.org/10.1124/pr.110.003129

Ding, S., and F. Sachs. 2000. Inactivation of P2X2 purinoceptors by divalent cations. *J. Physiol.* 522:199–214. http://dx.doi.org/10.1111/j.1469-7793.2000.t01-1-00199.x

Egan, T.M., D.S. Samways, and Z. Li. 2006. Biophysics of P2X receptors. *Pflugers Arch.* 452:501–512. http://dx.doi.org/10.1007/s00424-006-0078-1

Eickhorst, A.N., A. Berson, D. Cockayne, H.A. Lester, and B.S. Khakh. 2002. Control of $P2X_2$ channel permeability by the cytosolic domain. *J. Gen. Physiol.* 120:119–131.

Fisher, J.A., G. Girdler, and B.S. Khakh. 2004. Time-resolved measurement of state-specific P2X2 ion channel cytosolic gating motions. *J. Neurosci.* 24:10475–10487. http://dx.doi.org/10.1523/JNEUROSCI.3250-04.2004

He, M.L., H. Zemkova, T.A. Koshimizu, M. Tomić, and S.S. Stojilkovic. 2003. Intracellular calcium measurements as a method in studies on activity of purinergic P2X receptor channels. *Am. J. Physiol. Cell Physiol.* 285:C467–C479.

Housley, G.D., R. Kanjhan, N.P. Raybould, D. Greenwood, S.G. Salih, L. Järlebark, L.D. Burton, V.C. Setz, M.B. Cannell, C. Soeller, et al.

1999. Expression of the P2X(2) receptor subunit of the ATP-gated ion channel in the cochlea: implications for sound transduction and auditory neurotransmission. *J. Neurosci.* 19:8377–8388.

Khakh, B.S., and T.M. Egan. 2005. Contribution of transmembrane regions to ATP-gated P2X2 channel permeability dynamics. *J. Biol. Chem.* 280:6118–6129. http://dx.doi.org/10.1074/jbc.M411324200

Khakh, B.S., X.R. Bao, C. Labarca, and H.A. Lester. 1999. Neuronal P2X transmitter-gated cation channels change their ion selectivity in seconds. *Nat. Neurosci.* 2:322–330. http://dx.doi.org/10.1038/7233

Koshimizu, T., M. Tomić, M. Koshimizu, and S.S. Stojilkovic. 1998a. Identification of amino acid residues contributing to desensitization of the P2X2 receptor channel. *J. Biol. Chem.* 273:12853–12857. http://dx.doi.org/10.1074/jbc.273.21.12853

Koshimizu, T., M. Tomić, F. Van Goor, and S.S. Stojilkovic. 1998b. Functional role of alternative splicing in pituitary P2X2 receptor-channel activation and desensitization. *Mol. Endocrinol.* 12:901–913. http://dx.doi.org/10.1210/me.12.7.901

Koshimizu, T., M. Koshimizu, and S.S. Stojilkovic. 1999. Contributions of the C-terminal domain to the control of P2X receptor desensitization. *J. Biol. Chem.* 274:37651–37657. http://dx.doi.org/10.1074/jbc.274.53.37651

Koshimizu, T.A., K. Kretschmannova, M.L. He, S. Ueno, A. Tanoue, N. Yanagihara, S.S. Stojilkovic, and G. Tsujimoto. 2006. Carboxyl-terminal splicing enhances physical interactions between the cytoplasmic tails of purinergic P2X receptors. *Mol. Pharmacol.* 69:1588–1598. http://dx.doi.org/10.1124/mol.105.019802

Lynch, K.J., E. Touma, W. Niforatos, K.L. Kage, E.C. Burgard, T. van Biesen, E.A. Kowaluk, and M.F. Jarvis. 1999. Molecular and functional characterization of human P2X(2) receptors. *Mol. Pharmacol.* 56:1171–1181.

North, R.A. 2002. Molecular physiology of P2X receptors. *Physiol. Rev.* 82:1013–1067.

Parker, M.S., M.L. Larroque, J.M. Campbell, R.P. Bobbin, and P.L. Deininger. 1998. Novel variant of the P2X2 ATP receptor from the guinea pig organ of Corti. *Hear. Res.* 121:62–70. http://dx.doi.org/10.1016/S0378-5955(98)00065-3

Simon, J., E.J. Kidd, F.M. Smith, I.P. Chessell, R. Murrell-Lagnado, P.P. Humphrey, and E.A. Barnard. 1997. Localization and functional expression of splice variants of the P2X2 receptor. *Mol. Pharmacol.* 52:237–248.

Surprenant, A., F. Rassendren, E. Kawashima, R.A. North, and G. Buell. 1996. The cytolytic P2Z receptor for extracellular ATP identified as a P2X receptor (P2X7). *Science.* 272:735–738. http://dx.doi.org/10.1126/science.272.5262.735

Tyson, J.J., K.C. Chen, and B. Novak. 2003. Sniffers, buzzers, toggles and blinkers: dynamics of regulatory and signaling pathways in the cell. *Curr. Opin. Cell Biol.* 15:221–231. http://dx.doi.org/10.1016/S0955-0674(03)00017-6

Virginio, C., A. MacKenzie, F.A. Rassendren, R.A. North, and A. Surprenant. 1999. Pore dilation of neuronal P2X receptor channels. *Nat. Neurosci.* 2:315–321. http://dx.doi.org/10.1038/7225

Yan, Z., Z. Liang, T. Obsil, and S.S. Stojilkovic. 2006. Participation of the Lys313-Ile333 sequence of the purinergic P2X4 receptor in agonist binding and transduction of signals to the channel gate. *J. Biol. Chem.* 281:32649–32659. http://dx.doi.org/10.1074/jbc.M512791200

Yan, Z., S. Li, Z. Liang, M. Tomić, and S.S. Stojilkovic. 2008. The $P2X_7$ receptor channel pore dilates under physiological ion conditions. *J. Gen. Physiol.* 132:563–573. http://dx.doi.org/10.1085/jgp.200810059

Yan, Z., A. Khadra, S. Li, M. Tomic, A. Sherman, and S.S. Stojilkovic. 2010. Experimental characterization and mathematical modeling of P2X7 receptor channel gating. *J. Neurosci.* 30:14213–14224. http://dx.doi.org/10.1523/JNEUROSCI.2390-10.2010